SURROGATE MODELING OF VORTEX SHEDDING TURBINE IN LOW REYNOLDS NUMBER

Joshua Levin Kurniawan[1] & Matthew Hu[1]

[1]Faculty of Mechanical and Aerospace Engineering, Institut Teknologi Bandung, Jl. Ganesa No.10, Lb. Siliwangi, Kecamatan Coblong, Kota Bandung, Jawa Barat 40132, Indonesia

Abstract

Vortex shedding turbines (VST), a new type of wind turbine capable of generating renewable energy utilizing vortex-induced vibration (VIV) were recently found. To evaluate the potential and performance of a VST, accurate VIV prediction are necessary. VIV phenomena are usually formulated via complex fluid-structure interaction multi-physics problems, however, they are proven to be computationally heavy. On the other hand, experimental approaches are also impractical as it is very labor and equipment-intensive, hence an alternative is needed. Surrogate modeling emerges as a potential alternative. In this research, three models which are the linear regression, Gaussian Process Regression (GPR), and Neural Network (NN) methods are used to create surrogate models to predict the trend of vortex shedding frequency in a vortex shedding turbine on varying design variables. The design variables are freestream velocity (V), mast diameter (D), and model mass (m). The models achieved accuracy values ranging from 0.1770 to 0.2400 Root Mean Square Error and 0.60 to 0.84 R-squared values on validation data. The results indicate that the linear regression model could predict shedding frequency at best compared to GPR and NN. Furthermore, it is found that the vortex shedding frequency is linearly dependent on freestream velocity and mast diameter, and is inversely proportional to the model mass with gradients of 0.03, 0.0024, and -0.012 respectively.

Keywords: Vortex Shedding, Surrogate Modelling, Vortex Shedding Turbine, Renewable Energy, Vortex Induced Vibration

1. Introduction

In the search of sustainable and renewable energy generation, researchers and engineers have explored various innovative approaches to harnessing clean energy. A new concept of renewable energy generation is through wind energy, particularly through the vortex shedding phenomenon. Vortex shedding occurs when a fluid is flowing through a stationary bluff body, particularly a cylinder, resulting in a periodic separation of boundary layer [1]. Figure 1 shows the vorticity contour on a vortex shedding phenomenon that occurs on a cylinder. The Strouhal number usually parameterizes vortex shedding. Strouhal number is a proportionality constant between vortex shedding frequency (f_s) and diameter (D) with free-stream velocity (U). The Strouhal number describes the ratio of inertial forces due to the local acceleration (change of velocity with respect to time) to the inertial forces due to the convective acceleration (change of velocity to distance). This means at high Strouhal numbers, oscillations are prevalent, while at low Strouhal numbers, the oscillations are swept by the flow and subside [2]. Strouhal numbers are formulated in Equation 1 [3].

$$St = \frac{f_s \times D}{U} \tag{1}$$

If a flexible structure is experiencing vortex shedding, a vortex-induced vibration (VIV) phenomenon will occur. VIV refers to the cyclic oscillation of structures in response to the generation of periodic vortices due to vortex shedding caused by the flow [4]. This topic has been considerably studied,

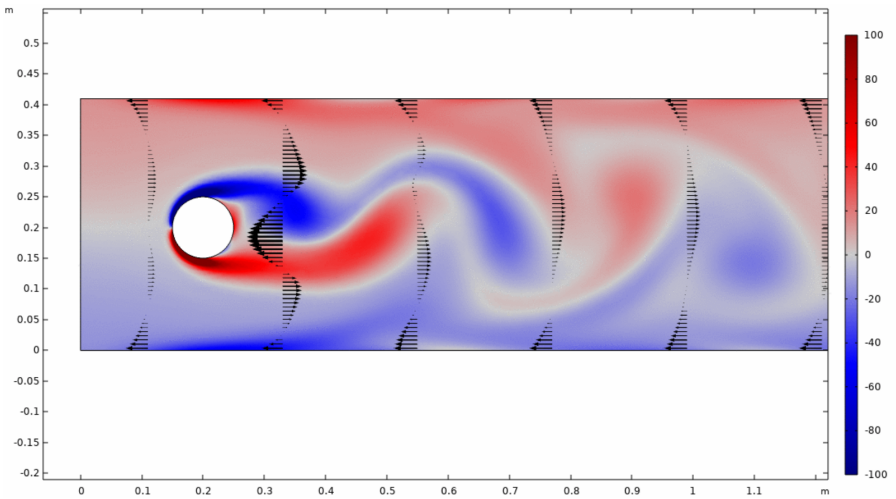

Figure 1 – Vorticity contour of vortex shedding in cylinder.

particularly in the offshore and aerospace fields. From a structural standpoint, VIV is known to be hazardous, leading to fatigue and damage to structures [5]. However, recent research has recognized the potential of harnessing the vibrations generated as a renewable energy source. A new type of wind turbine that utilizes the vortex-induced vibration phenomenon is the Vortex Shedding Turbines (VST).

The main components of VST consist of a fixed base, a core structure (that is the main structural component), a cylindrical mast that acts as the oscillator, and an energy generator such as an alternator. The typical VST are shown in Figure 2. The way VST mainly operates is by utilizing the oscillation of a cylindrical mast, which will create relative displacement that can be used for energy generation through induction or other means [4]. Therefore, displacement of the cylindrical mast proves to be an important parameter.

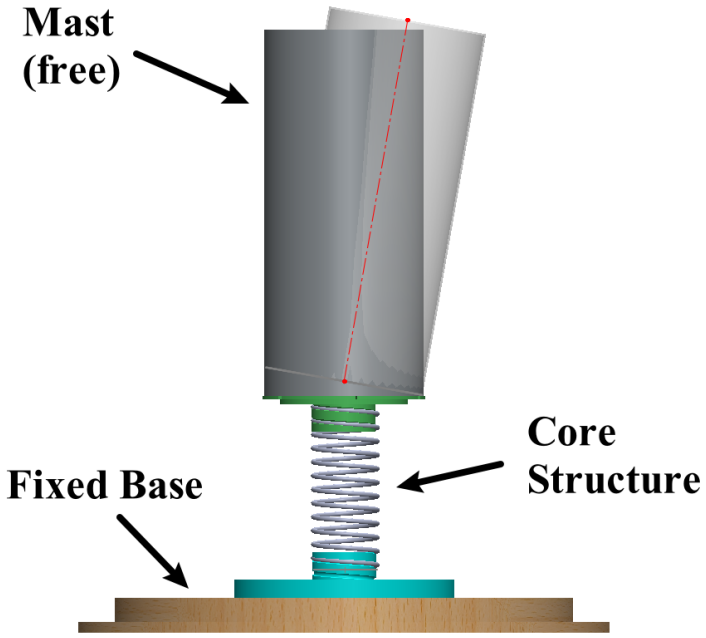

Figure 2 – Vortex shedding turbine components.

In comparison to the conventional counterparts, VST possess several advantages some of which are; less space requirements, omnidirectionality, cheaper and easier fabrication, greater life span, and many more [4]. Also, VST usually operates in lower wind speeds, meaning they can be used in more parts of the world. However, VST poses several challenges. To design an optimal VST, an

accurate prediction of VIV in the structure is needed.

A unique phenomenon that occurs in structures experiencing VIV is the resonance or lock-in phenomenon. Cylinder vibration near the shedding frequency of a stationary cylinder increases in strength of the shed vortices, hence the vortex shedding measured in a stationary cylinder is not a reliable predictor in a VIV motion [3]. To fully evaluate the VIV motion, a complete formulation of the fluid and structural dynamics is needed. This means a study using Fluid Structure Interaction (FSI) is needed. Several studies show that a complex FSI multi-physics modeling is capable of solving a vortex-induced vibration phenomenon. Cajas et al [6] developed a fluid-structure interaction in house code and successfully reproduced a satisfactory agreement between the numerical code with the experimental result. On the other hand, Hamdan et al [7] evaluated the performance of a VST using commercial software that facilitates two-way FSI numerical modeling, and validated the result with an experiment that is done in a wind tunnel on a smaller scale VST. Although both studies show a good agreement between the experiment and numerical modeling, the computational and labor costs for the numerical and experimental studies are very large.

To reduce computational and labor costs, surrogate modeling emerges as a promising candidate. Previous studies regarding surrogate modeling in Fluid-structure interaction cases include the research done by Arcones et al [8] where they developed an artificial neural network (ANN) as a basis of surrogate modeling specified for FSI implementation. The approach that is taken involves data generation using a conventional finite element model, model training using neural network architecture and finally implementing the created surrogate model. The model resulted in a decrease of simulation type without sacrificing accuracy. In addition to that, Wu et al [9] created an FSI design optimization framework that is used to improve the structural performance of a water brake. The surrogate management framework (SMF) is used to save time on the design of the water brake. The work resulted in a desirable decrease in von Mises stress from the baseline design, creating a time-efficient optimization procedure.

Although plenty of stationary cylinder vortex shedding studies are present, as mentioned before, VST motion cannot be interpreted using the still cylinder formulation. This paper therefore aims to predict the trend of the VIV properties, particularly in VSTs, using surrogate modeling in an effort to promote practicality, create time-efficient solvers, and observe the change of VIV frequency within the design space. Surrogate models will be developed to predict frequency tendencies based on the changes in the design parameters for small to mid-sized VSTs. In this research, the design variables that will be varied are the freestream velocity (V), mast diameter (D), and model mass (m). Freestream velocity and mast diameter are varied as the shedding properties are commonly dependent to them (seen in Equation 1), whereas mass proves to be an important parameter in determining the natural frequency of a system, which influence the total motion of a VST system. In a simplified single degree of freedom (SDOF) system, the natural frequency can be written as Equation 2 [10].

$$\omega_n = \sqrt{\frac{k}{m}}, \tag{2}$$

with ω_n is the natural frequency of the system, k is the stiffness of the system, and m is the mass of the system. This means generally mass is inversely proportional to the natural frequency of a system. A change in mass will influence the natural frequency of a system, thereby altering the system's motion tendencies.

Furthermore, the study will be limited at a low Reynolds number as nonlinearity and a larger degree of uncertainties become more apparent in the supercritical Reynolds regime. Several studies have been conducted in effort to find the trend of Strouhal Numbers in varying Reynolds numbers on a stationary cylindrical body. Aerodynamic flows in cylindrical objects are categorized into three regimes, namely the subcritical ($Re \leq 2\times10^5$), critical ($2\times10^5 < Re \leq 6\times10^5$), and the supercritical regime ($Re > 6\times10^5$) [3][11]. Below the subcritical regime, it is found that the Strouhal number is function of the Reynolds number, with an average Strouhal number of approximately 0.21 [12]. However above Reynolds number of 2×10^5, they are independent of Reynolds number [13], making the prediction of vortex shedding frequency harder in the high Reynolds regime.

2. Experimental Setup and Data

To obtain the training data, VST models are constructed and tested in a closed-loop wind tunnel. The main interest is to capture the frequency of the VST model in diverse design points. The wind closed-loop wind tunnel section can be seen in Figure 3.

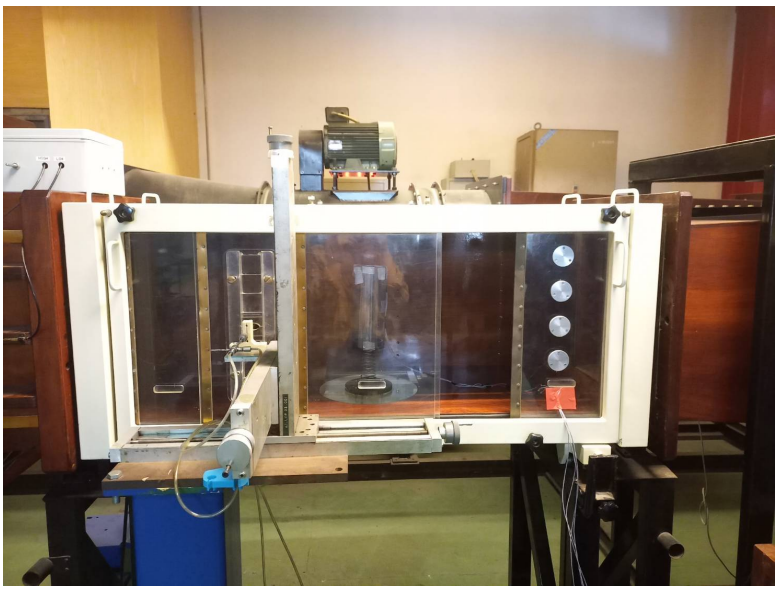

Figure 3 – Closed loop wind tunnel test section.

The test model consists of 4 main parts, namely the base, spring (main structural component), cylindrical mast, and sensor. To obtain the VST motion data, an inertial measurement unit (IMU) is used. The MPU-6050 GY-521 sensor module is used. The MPU-6050 is equipped with a 3-axis accelerometer which is capable of measuring linear acceleration in the X, Y, and Z orientation, and a gyroscope that can obtain the angular velocity in the 3-axis as well. The IMU module is placed inside the test specimen. The test model is shown in Figure 4.

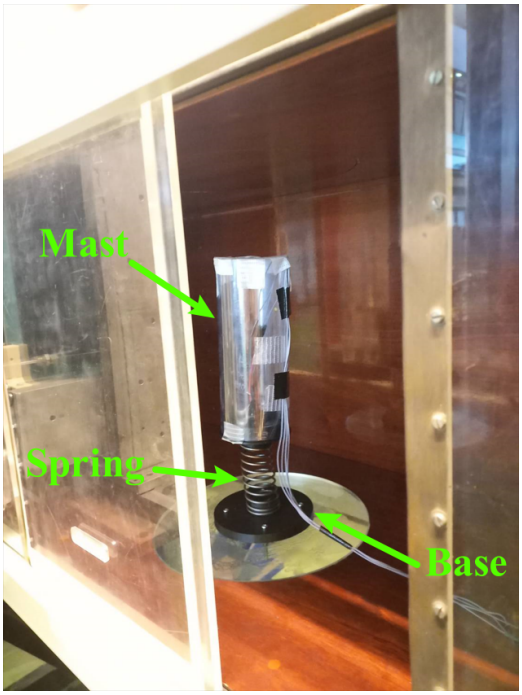

Figure 4 – Experimental test model.

The experiment will be divided into two experiments each consisting of 27 design points. The design variables that are varied are the freestream velocity (V), mast diameter (D), and model mass (m)

which is sampled using Latin hypercube sampling (LHS). Freestream velocity is varied by changing the compressor rate which corresponds to the volume of fluid flowed, mast diameter is adjusted by changing the mast sample (see Figure 5), where the model mass is modified by applying a ballast to give additional weight to the system.

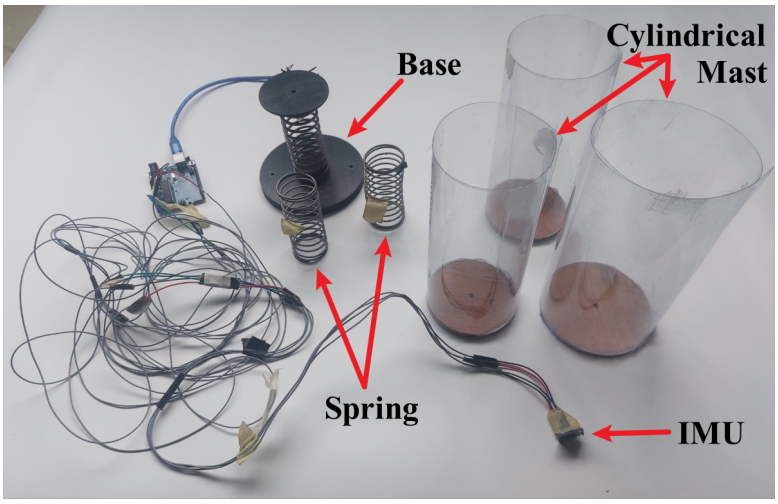

Figure 5 – Unassembled experimental test model.

The experiment will be done in the low Reynolds number region, which ranges between 4219, to 98087, the Reynolds number variation can be seen in Figure 6. The experimental result and sampling points for experiments 1 and 2 can be seen in Figure 7 and Figure 8 respectively.

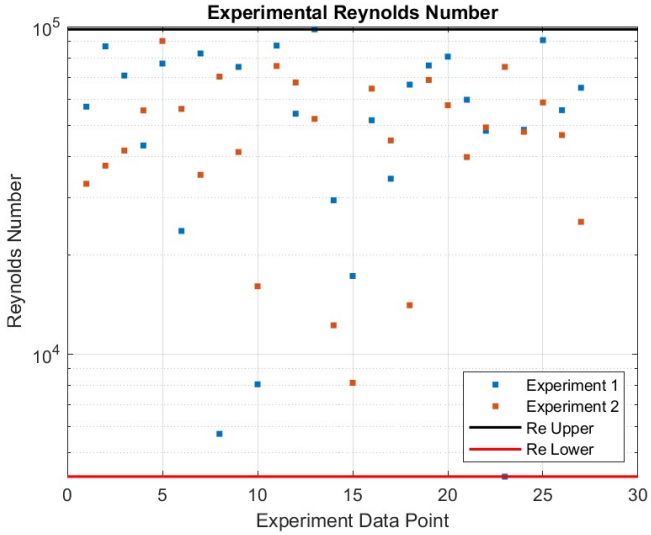

Figure 6 – Experimental Reynolds number variations.

To accurately extract the frequency of the VST, the data on acceleration and angular velocity obtained by the IMU is analyzed using the persistence spectrum. The persistence spectrum is presented in a power-frequency histogram which shows the percentage of time a given frequency is present in a signal. The spectrogram of the signal is computed in a specified leakage, time resolution, and overlap. Then the power and frequency values are partitioned into 2-D bins and the histogram of the power spectrum for each time value. The power spectrum is the distribution of power contained within a signal over the frequency domain. To compute the time-dependent spectrum of a signal, the obtained signal will be divided into segments (to avoid calculating large Fourier transforms) that will be analyzed using a short-time Fourier transform. The sample of the persistence spectrum analysis can be seen in Figure 9.

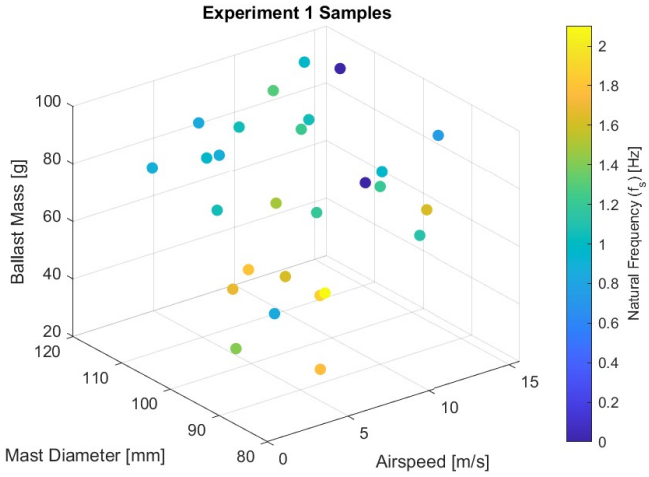

Figure 7 – Experiment 1 samples plot.

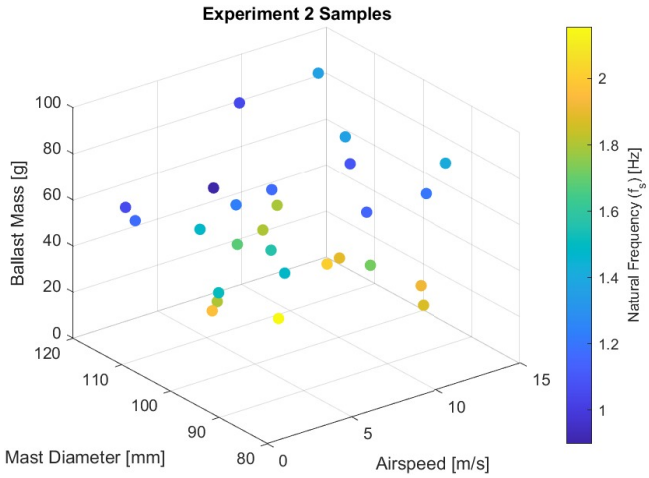

Figure 8 – Experiment 2 samples plot.

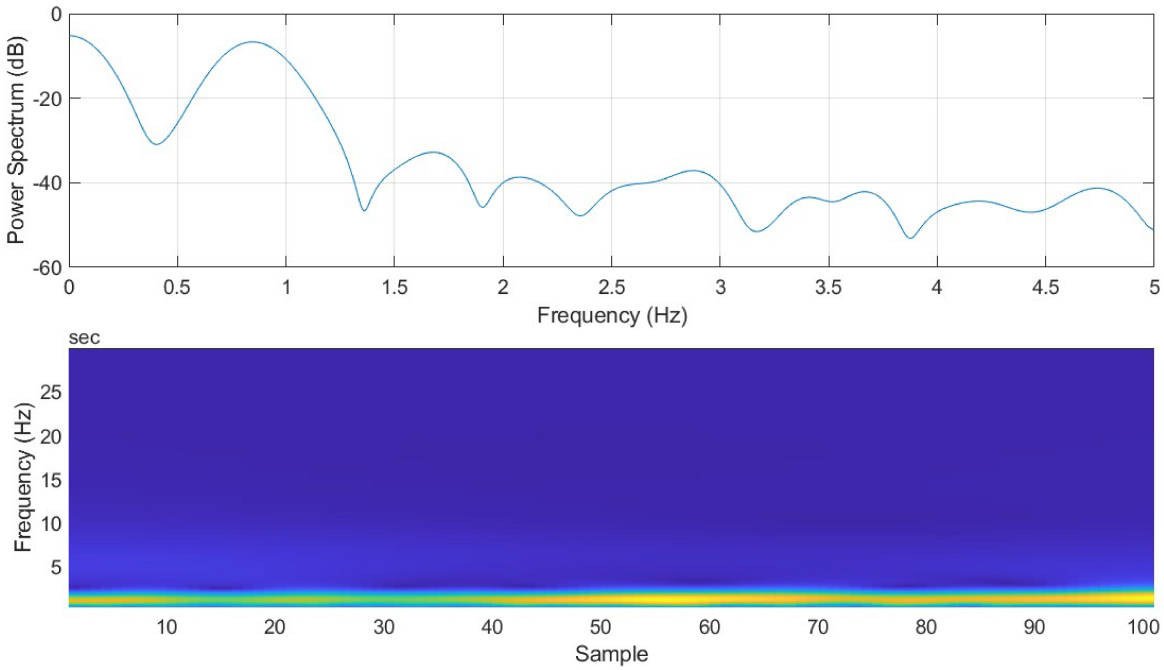

Figure 9 – Power spectrum (top) and persistence spectrum (bottom).

3. Prediction Models

In this research, a set of supervised learning methods will be used to create surrogate models to predict the fluid-structure interaction response, specifically vortex shedding frequency. The surrogate models will be constructed using several methods with different levels of flexibility and interpretability, including linear regression, Gaussian Process Regression (GPR), and neural networks.

3.1 Linear Regression Models

A linear regression model is one type of statistical model that is able to predict the value of a dependent variable with the assumption that it is based on one or more independent variables [14]. In general, linear regression is able to create a prediction based on the relation between a response Y with the predictor X.

$$Y \approx \beta_0 + \beta_1 X, \tag{3}$$

with β_0 and β_1 represents the unknown intercept and slope constants, also called coefficients. Let there be n number of samples, the value of estimated coefficients ($\hat{\beta}_0$ and $\hat{\beta}_1$) will be evaluated such that it can minimize the least square values.

$$\begin{aligned} \hat{\beta}_1 &= \frac{\Sigma_{i=1}^{n}(X_i - \overline{X})(Y_i - \overline{Y})}{\Sigma_{i=1}^{n}(X_i - \overline{X})^2}, \\ \hat{\beta}_0 &= \overline{Y} - \hat{\beta}_1 \overline{X}, \end{aligned} \tag{4}$$

with $\overline{Y} = \frac{1}{n}\Sigma_{i=1}^{n} Y_i$ and $\overline{X} = \frac{1}{n}\Sigma_{i=1}^{n} X_i$, also called the sample means. Additionally, the terms of X can be modified. Specifically, for this research, the terms used are linear and interactions. Linear terms mean that the system only consists of an intercept and linear terms of each predictor. On the other hand, for interactions terms, the model contains intercept and linear terms, but also with the addition of pairs of distinct predictors, which allows for more accurate predictions [15].

3.2 Gaussian Process Regression Models

Gaussian Process Regression (GPR) is a probabilistic model in machine learning that is nonparametric and relies on kernels [16]. In general, GPR has a high flexibility but is harder to interpret compared to the linear regression model. Consider a linear regression model as follows.

$$Y \approx X^T \hat{\beta} + \varepsilon, \;\; \varepsilon \sim N(0, \sigma^2), \tag{5}$$

where $N(0,\sigma^2)$ as the Gaussian distribution with zero mean and σ^2 variance . The Gaussian process model predicts the response by using a set of latent variables ($f(X_i)$) from the Gaussian process and a set of explicit basis functions h. Hence, the response Y can be modeled in vector form as follows.

$$P(Y|f(X),X) \sim N(Y|H\beta + f, \sigma^2 I), \tag{6}$$

where H is $h(X_i)$ in vector form. In this research, the basis function of the prior mean Gaussian process regression model function is constant. The Gaussian process model interprets the covariance function between two latent variables $f(X_i)$ and $f(X_j)$. This covariance function ($k(x_i, x_j|\theta)$) is defined by kernel functions vector (θ). Let the kernel parameters be defined by the standard deviation σ_f and the characteristic length scale σ_l, then the parametrization of kernel vector θ can be described as Equation 7 [16].

$$\theta_1 = \log \sigma_l, \;\; \theta_2 = \log \sigma_f. \tag{7}$$

Specifically, in this research, the used kernel functions will be the rational quadratic and exponential kernel. In the case of the rational quadratic kernel, the kernel function is defined as a function that consists of positive-valued scale-mixture parameter α, as written in Equation 8.

$$k(X_i, X_j|\theta) = \sigma_f^2 \left(1 + \frac{(X_i - X_j)^T (X_i - X_j)}{2\alpha\sigma_l^2}\right). \tag{8}$$

On the other hand, for the exponential kernel, the kernel function is defined as Equation 9.

$$k(X_i, X_j|\theta) = \sigma_f^2 e^{-\frac{\sqrt{(X_i - X_j)^T (X_i - X_j)}}{\sigma_l}}. \tag{9}$$

In this research, various kernel functions will be utilized for the Gaussian Process Regression (GPR) method to evaluate the effect of the kernel function on the fitness of the model.

3.3 Neural Networks

A neural network refers to a computational model that consists of a collection of interconnected nodes that process and learn from data. Neural network models typically have high flexibility, which can vary depending on the number of active layers and the size of each corresponding layer. In this research, the model used is a fully connected, feedforward neural network.
The surrogate modeling process involves connecting the predictor data to the first layer. For each subsequent layer, the inputs are connected to the previous layer. Each layer provides a weight matrix and bias vector for the inputs. Generally, the number of fully connected layers and their size increase the model's flexibility.

4. Surrogate Model Training and Prediction Result

The experimental results that have been obtained will be used to train a surrogate model using several methods, including linear regression, Gaussian Process Regression (GPR), and neural networks. The trained model will then be interpreted using the partial dependence analysis.

4.1 Model Setup

In general, this research will involve three main modeling methods: linear regression, GPR, and neural networks. Each model will contain several different hyperparameters to investigate the impact of these parameters on the results. For linear regression, the terms used will vary between linear and interaction. The linear regression setup are shown in Table 1.

Table 1 – Linear regression setup.

Model	Linear	Linear (Interactions)	Linear (Robust)
Terms	linear	interactions	linear
Robustness	off	off	on

For GPR, the kernel function will vary between Rational Quadratic and Squared Exponential, which is detailed in Table 2. In this case, an isotropic kernel will be used for each scenario, with the basic function set to be constant. An isotropic kernel in this case refers to the kernel function properties which has the same length scale for all input features [16].

Table 2 – GPR setup.

Model	GPR (Rational Quadratic)	GPR (Rational Quadratic)
Basis Function	constant	constant
Kernel Function	rational quadratic	exponential
Kernel Type	isotropic	isotropic

Finally, for the neural network model, the number of layers will be varied between one and two, with different sizes, as tabulated in Table 3.

Table 3 – Neural network setup.

Model	Neural Network (Narrow)	Neural Network (Wide)	Neural Network (Bilayer)
Number of connected layer	1	1	2
First layer size	10	35	30
Second layer size	-	-	30
Activation	ReLU	ReLU	ReLU

4.2 Validation and Test Result

Each experiment consists of 27 training data points and 9 test data points. Additionally, the training data will be cross-validated with 3 folds to test the robustness of the models. The goal of the surrogate model is to create a predictive model of vortex shedding frequency generation as the result of fluid-structure interaction on a vortex shedding turbine. In this case, the model will predict the vortex shedding frequency (f_{shed}) as a function of freestream velocity (V), mast's diameter (D), and the vortex shedding turbine model mass (m).

$$f_{shedding} = F(V, D, m) \tag{10}$$

The training results will be validated and tested by evaluating the Root Mean Square Error (RMSE) and R^2 value. These metrics are commonly used to evaluate the performance of trained surrogate models [17]. In this case, RMSE is calculated using Equation 11.

$$RMSE = \sqrt{\frac{1}{n}\Sigma_{i=1}^{n}|F_i - A_i|^2}, \tag{11}$$

with F as the predicted data array and A as the actual data array. This value measures the average difference between a model's predicted values and the actual values. Additionally, to measure the proportion of the variance in the response variable, the coefficient of determination (R^2) is introduced, as mentioned in Equation 12.

$$R^2 = 1 - \frac{\Sigma e^2}{\Sigma T^2}, \tag{12}$$

Table 4 – RMSE result.

Model	Experiment 1		Experiment 2	
	Validation	Test	Validation	Test
Linear	0.1880	0.2298	0.1770	0.1825
Linear (Interactions)	0.2400	0.2185	0.1722	0.1808
Linear (Robust)	0.1808	0.2009	0.1752	0.1839
GPR (Rational Quadratic)	0.2017	0.2153	0.1861	0.1855
GPR (Exponential)	0.2096	0.2616	0.1761	0.1855
Neural Network (Narrow)	0.1909	0.2528	0.1857	0.2168
Neural Network (Wide)	0.1903	0.2520	0.1859	0.2179
Neural Network (Bilayer)	0.19504	0.2569	0.1823	0.1923

with Σe^2 as the sum of squared error and ΣT^2 as the sum of squared total. After training the model, the result as tabulated in Table 4 and Table 5 for RMSE and R-squared value respectively are obtained.

Table 5 – Coefficient of determination (R^2).

Model	Experiment 1		Experiment 2	
	Validation	Test	Validation	Test
Linear	0.75	0.64	0.83	0.77
Linear (Interactions)	0.60	0.68	0.84	0.77
Linear (Robust)	0.77	0.73	0.83	0.77
GPR (Rational Quadratic)	0.71	0.69	0.84	0.76
GPR (Exponential)	0.69	0.54	0.82	0.70
Neural Network (Narrow)	0.74	0.57	0.82	0.68
Neural Network (Wide)	0.75	0.57	0.82	0.67
Neural Network (Bilayer)	0.73	0.55	0.79	0.74

The results, as tabulated in Table 4 and Table 5, indicate how well the models predict shedding frequency as a function of the varied variables (V, D, and m). A lower RMSE value suggests that the model has a lower absolute error on the given data, while a high R-squared value indicates how well the model explains the variance in the data. From the result table, for the same model, experiment 2 shows a higher accuracy prediction compared to experiment 1.

Notably, higher flexibility models, such as Gaussian Process Regression (GPR) and neural networks, generally show higher RMSE and lower R-squared values compared to the linear regression model for both validation and test data on both experimental data sets. This can be observed in Figure 10, where the predicted response values for the linear regression model are closer to the true response values, evidenced by the scattered points being nearer to the line. This property indicates that the model makes accurate predictions across different response values. The result that indicates the linear regression model provides the best fit to the data suggests a linear relationship between the vortex shedding frequency and the variables of freestream velocity, mast diameter, and model mass. Furthermore, each model's accuracy can be evaluated using response plots, allowing observation of how much the predicted data deviate from the actual data. These plots visually demonstrate the relationship between the predicted and actual values, making it easier to assess the performance and reliability of each model.

Figure 11, with response value in Hertz, shows the response plot of each linear model for both experiments. The plots show that the linear (robust) model provides more overall accuracy in predicting the shedding frequency than the other two models. This demonstrates how the robust objective function can make the trained model less sensitive to outliers by assigning lower weights to the outlier data.

On the other hand, for the GPR response plot, as seen in Figure 12 (with response value in Hertz), the two models show no significant difference in terms of accuracy. This indicates that for Gaussian process regression, the kernel function choice between Rational Quadratic and Exponential yields comparable accuracy in predicting the shedding frequency.

In the response plots for the neural network models, as depicted in Figure 13 (with response value in Hertz), it's evident that the number and size of the connected layers impact the model's accuracy. In this scenario, increasing the size of the layer (for a single connected layer) improves accuracy. This trend persists with the addition of fully connected layers. Compared to a single active layer, bilayered neural networks demonstrate improved predictive capability.

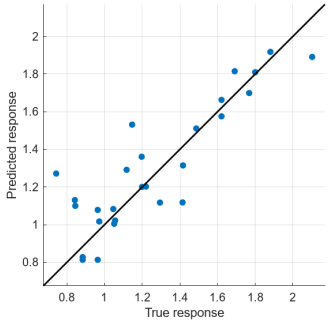

(a). Linear (robust)
Experiment 1

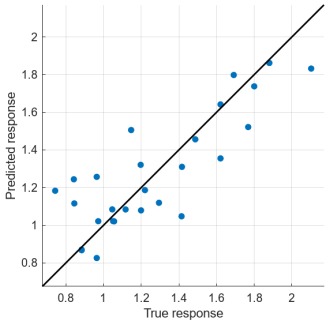

(b). GPR (rational quadratic)
Experiment 1

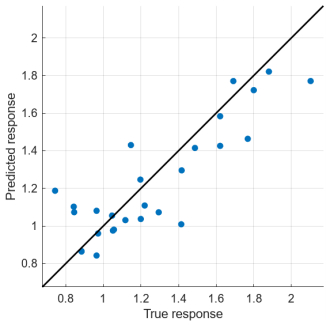

(c). Neural network (wide)
Experiment 1

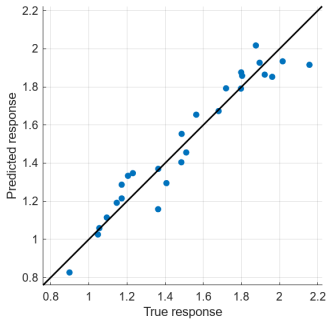

(d). Linear (robust)
Experiment 2

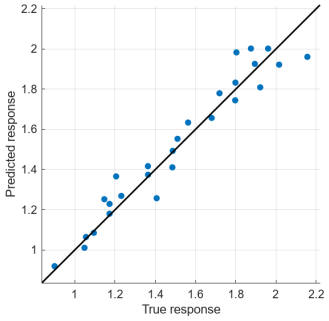

(e). GPR (rational quadratic)
Experiment 2

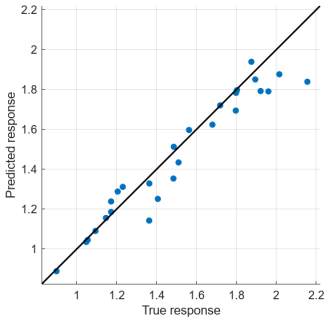

(f). Neural network (wide)
Experiment 2

Figure 10 – Predicted vs. actual plots.

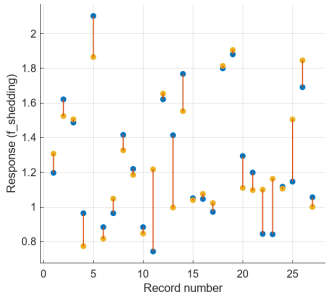

(a). Linear
Experiment 1

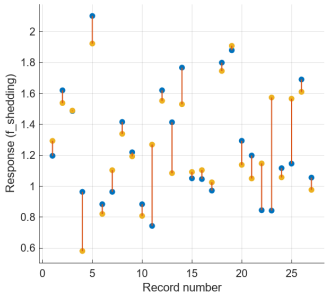

(b). Linear (interactions)
Experiment 1

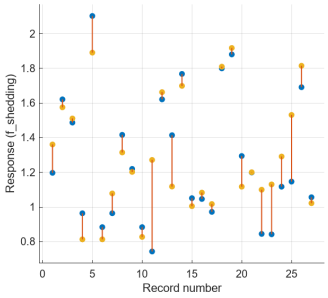

(c). Linear (robust)
Experiment 1

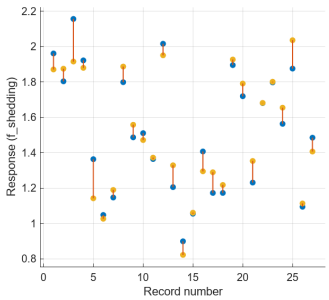

(d). Linear
Experiment 2

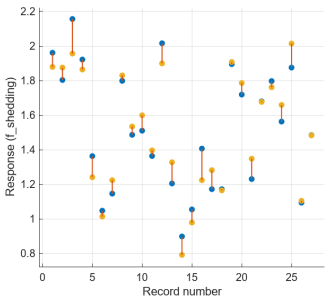

(e). Linear (interactions)
Experiment 2

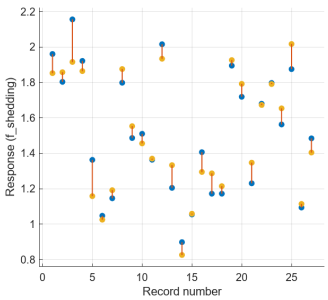

(f). Linear (robust)
Experiment 2

Figure 11 – Linear models response plots.

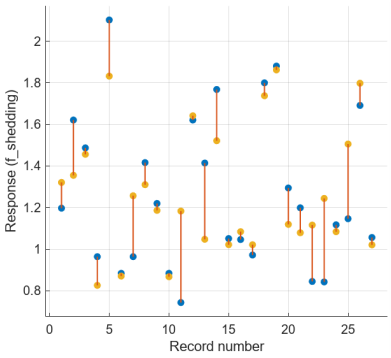

(a). GPR (rational quadratic) Experiment 1

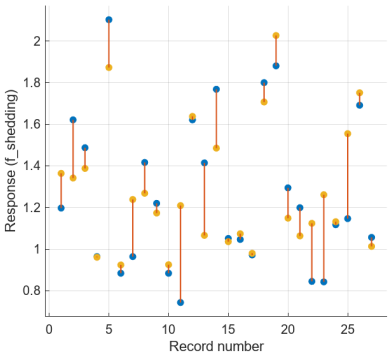

(b). GPR (Exponential) Experiment 1

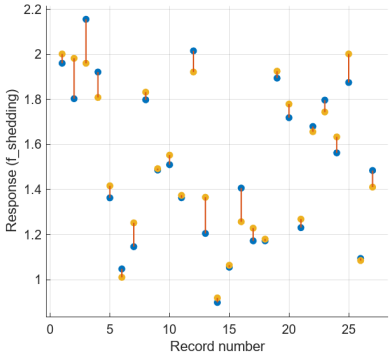

(c). GPR (rational quadratic) Experiment 2

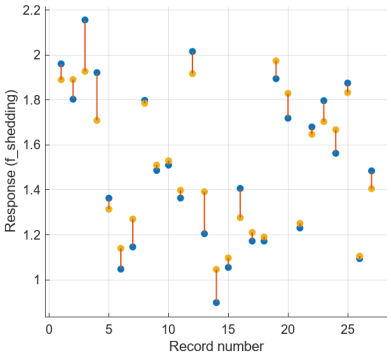

(d). GPR (Exponential) Experiment 2

Figure 12 – GPR models response plots.

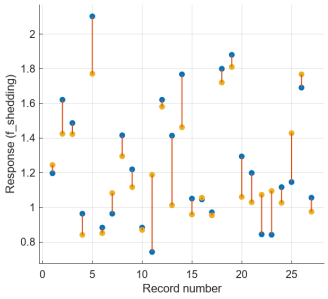

(a). Neural network (narrow) Experiment 1

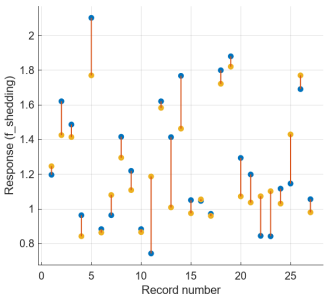

(b). Neural network (wide) Experiment 1

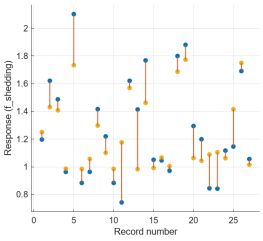

(c). Neural network (bilayer) Experiment 1

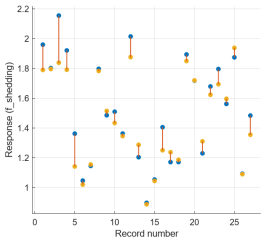

(d). Neural network (narrow) Experiment 2

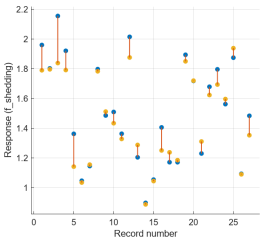

(e). Neural network (wide) Experiment 2

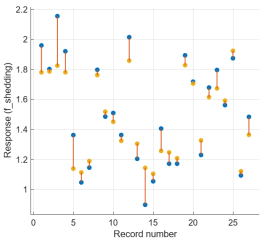

(f). Neural network (bilayer) Experiment 2

Figure 13 – Neural network models response plots.

4.3 Interpretation

In this section, we will leverage the linear (robust) model, which provides the most accurate prediction of the vortex shedding frequency, to interpret the behavior of the model. Utilizing a linear model offers greater interpretability compared to GPR and neural networks [18]. Specifically, we will examine the partial dependency of each predictor variable and the predicted response [19]. Our focus will be on the first experiment's training data.

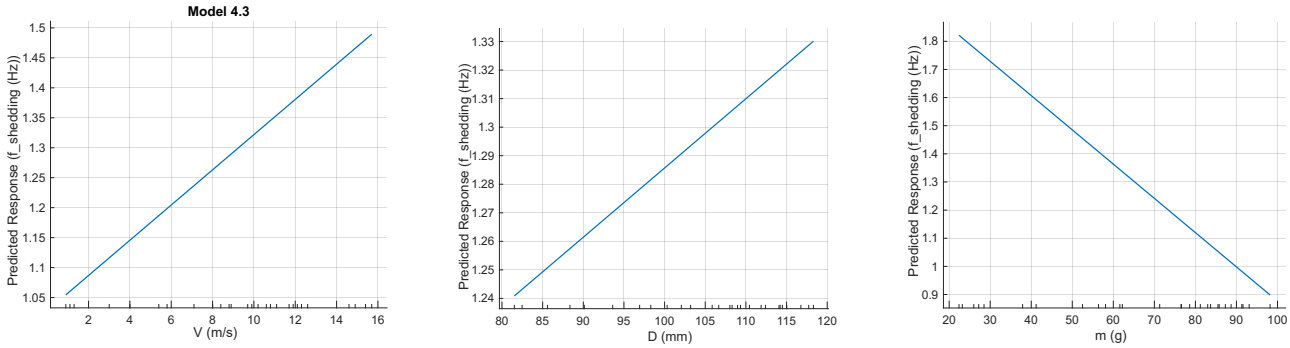

(a). Freestream velocity (b). Mast's diameter (c). Model mass

Figure 14 – Partial dependency of predictor variable and predicted shedding frequency.

Using the partial dependency plot illustrated in Figure 14, we can analyze the effect of altering the parameters (V, D, and m) on the vortex shedding frequency based on the data. The results indicate that as the freestream velocity increases, the expected vortex shedding frequency also increases. Similarly, the mast's diameter affects the shedding frequency, with an increase in diameter leading to a higher shedding frequency. In contrast to the direct proportionality observed with freestream velocity and mast diameter, the mass of the model inversely affects the vortex shedding frequency, with an increase in mass resulting in a decrease in frequency. The effect of each predictor variable on vortex shedding frequency as the result of fluid-structure interaction can be seen in Table 6.

Table 6 – Effect of increasing vortex shedding turbine operational variables on vortex shedding frequency.

Increased variable	**Freestream velocity**	**Mast's diameter**	**Model mass**
Vortex shedding frequency	Increasing (gradient of 0.03)	Increasing (gradient of 0.0024)	Decreasing (gradient of -0.012)

In an SDOF system, vibrations that is under harmonic excitation will vibrate under the frequency of the excitation [10]. VIV motions are known to be excited by the oscillatory shedding vortices force. Although in practice, the shedding force depends on the cylinder motion (the force excited in VIV is not the same as vortex shedding in a stationary cylinder), by assuming the VST as an SDOF system excited by harmonic vortex shedding force, the VST motion can be estimated with the Strouhal number correlation. Since the research is conducted in the subcritical Reynolds regime, the Strouhal number throughout the design points is ≈ 0.21. Examining equation 1, it can be seen that the vortex shedding frequency is linearly dependent on the freestream velocity, which follows a similar trend to the correlation found in this research, showing a linear dependency with a gradient of approximately 0.025. This means as freestream velocity increases, the tendency of a cylinder to oscillate at a higher frequency increases. Using the Strouhal equation, it is found that the vortex shedding frequency is inversely proportional to the diameter, which differs to what is found in this research. This may occur due to the presence of lock-in phenomenon that is unpredictable using the stationary cylinder vortex shedding Strouhal number [20]. As the diameter of the mast increases, the aerodynamic forces become more dominant, meaning the oscillation amplitude will increase under the same given structural stiffness. This means as the diameter increases, the VIV frequency will shift closer to the resonance frequency, which is unforeseeable using the still cylinder vortex shedding motion. From the research, it is found that generally the vortex shedding frequency will increase

as the mast diameter increases. In addition to that, generally mass is inversely proportional to the natural frequency of a system as seen in Equation 2. Therefore, the system will tend to vibrate at a lower frequency, which corresponds to the decreased natural frequency in the increase of mass. This finding is inline with the finding in the research, where when the model mass is increased, the VST tends to oscillate at a lower frequency.

5. Conclusion

This research has demonstrated surrogate modeling of vortex shedding frequency resulting from fluid-structure interaction in a vortex shedding turbine. In this study, experiments were conducted in a closed-loop wind tunnel using a scaled-down vortex shedding turbine model, and surrogate models were developed using linear regression, Gaussian Process Regression (GPR), and neural network methods. The models exhibited accuracies ranging from 0.1770 to 0.2400 RMSE and 0.60 to 0.84 R-squared values on validation data. The results indicated that a robust linear regression model could predict shedding frequency with the highest accuracy. Additionally, partial dependency analysis showed that vortex shedding frequency resulting from fluid-structure interaction is directly proportional to both freestream velocity and mast diameter, but inversely proportional to the model mass. These findings can assist in the design process of vortex shedding turbines, which involve complex fluid-structure interaction phenomena, by aiding in the determination of design parameters for predicting shedding frequency.

6. Contact Author Email Address

For additional information regarding the paper, feel free to contact the authors using the following email address:

- joshualevinkurniawan@gmail.com
- 11matthew.hu@gmail.com

7. Copyright Statement

References

[1] Houghton, E.L. *Aerodynamics for Engineering Students*. Elsevier Science, 2012.

[2] Katopodes, Nikolaos D. *Free-surface flow: environmental fluid mechanics*. Butterworth-Heinemann, 2018.

[3] Blevins, Robert D. Models for Vortex-Induced Vibration of Cylinders Based on Measured Forces. *Journal of Fluids Engineering*, Vol. 131, 2009.

[4] Villarreal, DJ Yáñez and SL, Vortex Bladeless. VIV resonant wind generators. *Vortex Bladeless SL*, 2018.

[5] Zou, Xing and Xie, Botao and Zang, Zhipeng and Chen, Enbang and Hou, Jing. Vortex-Induced Vibration and Fatigue Damage Assessment for a Submarine Pipeline on a Sand Wave Seabed. *Journal of Marine Science and Engineering*, Vol. 11, 2023.

[6] Cajas, Juan C and Houzeaux, Guillaume and Yáñez, David J and Mier-Torrecilla, Mónica. SHAPE project Vortex Bladeless: Parallel multi-code coupling for fluid-structure interaction in wind energy generation. *Adv. Comput. Eur*, Vol. 12, pp 1-6, 2016.

[7] Hamdan, Hasan and Dol, Sharul Sham and Gomaa, Abdelrahman Hosny and Tahhan, Aghyad Belal Al and Al Ramahi, Ahmad and Turkmani, Haya Fares and Alkhedher, Mohammad and Ajaj, Rahaf. Experimental and Numerical Study of Novel Vortex Bladeless Wind Turbine with an Economic Feasibility Analysis and Investigation of Environmental Benefits. *Energies*, Vol. 17, 2024.

[8] Andrés Arcones, Daniel and Ellath Meethal, Rishith and Obst, Birgit and Wüchner, Roland. Neural Network-Based Surrogate Models Applied to Fluid-Structure Interaction Problems. *15th World Congress on Computational Mechanics (WCCM-XV) and 8th Asian Pacific Congress on Computational Mechanics (APCOM-VIII)*, 2022.

[9] Wu, Michael C. H. and Kamensky, David and Wang, Chenglong and Herrema, Austin and Xu, Fei and Pigazzini, Marco Simone and Verma, Aekaansh and Marsden, Alison and Bazilevs, Yuri and Hsu, Ming-Chen. Optimizing fluid–structure interaction systems with immersogeometric analysis and surrogate modeling: Application to a hydraulic arresting gear. *Computer Methods in Applied Mechanics and Engineering*, Vol. 316, pp 668-693, 2017.

[10] Inman, Daniel J. *Engineering Vibration*. Prentice Hall Englewood Cliffs, NJ, 2014.

[11] Roshko, Anatol. On the development of turbulent wakes from vortex streets. *NACA Report, Printed in USA*, Vol. 1191, 1954.

[12] White, Frank M and Ng, CO and Saimek, S. *Fluid mechanics*, McGraw-Hill, cop., 2021.

[13] Ellingsen, Øyvind Mortveit and Amandolese, Xavier and Hémon, Pascal. In wind tunnel the reproduction of vortex shedding behind circular cylinders at high Reynolds number regimes is incomplete. *12th International Conference on Flow-Induced Vibrations*, 2022

[14] Trevor Hastie, Robert Tibshirani, Jerome H. Friedman. *The Elements of Statistical Learning: Data Mining, Inference, and Prediction*. Vol. 2, Springer, 2009.

[15] M. Lunt. Introduction to Statistical Modelling 2: Categorical Variables and Interactions in Linear Regression. *Rheumatology*, Vol. 54, issue 7, pp 1141-1144, 2015. DOI: 10.1093/rheumatology/ket172

[16] C. E. Rasmussen. *Gaussian Processes for Machine Learning*. MIT Press Cambridge, MA, USA, 2006.

[17] Gareth James, Daniela Witten, Trevor Hastie, Robert Tibshirani, and others. *An Introduction to Statistical Learning*, Vol. 112, Springer, 2013.

[18] Andriy Burkov. *Machine Learning Engineering*. Vol. 1, True Positive Incorporated, Montreal, QC, Canada, 2020.

[19] Alex Goldstein, Adam Kapelner, Justin Bleich, Emil Pitkin. Peeking Inside the Black Box: Visualizing Statistical Learning with Plots of Individual Conditional Expectation. *Journal of Computational and Graphical Statistics*, Vol. 24, No. 1, pages 44-65, Taylor & Francis, 2015.

[20] Williamson, Charles HK and Roshko, Anatol. Vortex formation in the wake of an oscillating cylinder. *Journal of fluids and structures*, Vol. 2, pp 355-381, 1988